

The NEWFIRM Medium-Band Survey: Filter Definitions and First Results

Pieter G. van Dokkum^{1,2}, Ivo Labbé³, Danilo Marchesini¹, Ryan Quadri⁴, Gabriel Brammer¹, Katherine E. Whitaker¹, Mariska Kriek⁵, Marijn Franx⁴, Gregory Rudnick⁶, Garth Illingworth⁷, Kyoung-Soo Lee¹, Adam Muzzin¹

ABSTRACT

Deep near-infrared imaging surveys allow us to select and study distant galaxies in the rest-frame optical, and have transformed our understanding of the early Universe. As the vast majority of K - or IRAC-selected galaxies is too faint for spectroscopy, the interpretation of these surveys relies almost exclusively on photometric redshifts determined from fitting templates to the broad-band photometry. The best-achieved accuracy of these redshifts $\Delta z/(1+z) \gtrsim 0.06$ at $z > 1.5$, which is sufficient for determining the broad characteristics of the galaxy population but not for measuring accurate rest-frame colors, stellar population parameters, or the local galaxy density. We have started a near-infrared imaging survey with the NEWFIRM camera on the Kitt Peak 4m telescope to greatly improve the accuracy of photometric redshifts in the range $1.5 \lesssim z \lesssim 3.5$. The survey uses five medium-bandwidth filters, which provide crude “spectra” over the wavelength range $1 - 1.8 \mu\text{m}$ for all objects in the $27'6 \times 27'6$ NEWFIRM field. In this first paper, we illustrate the technique by showing medium band NEWFIRM photometry of several galaxies at $1.7 < z < 2.7$ from the near-infrared spectroscopic sample of Kriek et al. (2008). The filters unambiguously pinpoint the location of the redshifted Balmer break in these galaxies, enabling very accurate redshift measurements. The full survey will provide similar data for ~ 8000 faint K -selected galaxies at $z > 1.5$ in the COSMOS and AEGIS fields. The filter set also enables efficient selection of exotic objects such as high redshift quasars, galaxies dominated by emission lines, and very cool brown dwarfs; we show that late T and candidate “Y” dwarfs could be identified using only two of the filters.

Subject headings: galaxies: distances and redshifts — galaxies: high-redshift

1. Introduction

It has become clear that the Universe at $1.5 < z < 3.5$ saw a much greater diversity of galaxies than the Universe today. This epoch is often characterized as

one of rapid change, as many galaxies were experiencing strong and presumably short-lived star formation (Steidel et al. 1996; Blain et al. 2002), significant merging activity, and rapid black hole growth (e.g., Daddi et al. 2007). At the same time a substantial population of quiescent galaxies already existed (e.g., Kriek et al. 2006). These galaxies have spectra characterized by strong Balmer or 4000 \AA breaks and no detected $H\alpha$ emission. They also have very compact morphologies, which implies they must undergo significant subsequent evolution (e.g., Trujillo et al. 2006; Cimatti et al. 2008; van Dokkum et al. 2008).

Given the diversity and rapid changes in the galaxy population at this epoch, it is important to secure and study large, uniformly selected samples of galaxies at $1.5 < z < 3.5$ in a homogeneous way. Unfortunately it is difficult to obtain such samples, as familiar rest-frame optical spectral features are shifted into the

¹Department of Astronomy, Yale University, New Haven, CT 06520-8101.

²Visiting Astronomer, Kitt Peak National Observatory, National Optical Astronomy Observatory, which is operated by the Association of Universities for Research in Astronomy (AURA) under cooperative agreement with the National Science Foundation.

³Carnegie Observatories, Pasadena, CA 91101.

⁴Sterrewacht Leiden, Leiden University, NL-2300 RA Leiden, Netherlands.

⁵Department of Astrophysical Sciences, Princeton University, Princeton, NJ 08544.

⁶Department of Physics and Astronomy, University of Kansas, Lawrence, KS 66045.

⁷UCO/Lick Observatory, University of California, Santa Cruz, CA 95064.

near-infrared. As a consequence, most studies of high redshift galaxies have focused on blue star forming galaxies, as they are relatively bright at observed optical (rest-frame ultra-violet) wavelengths (e.g., Steidel et al. 1996, 1999). Although this approach is very efficient, it misses galaxies that are relatively red: as shown in van Dokkum et al. (2006) the majority of galaxies with masses $> 10^{11} M_{\odot}$ at $2 < z < 3$ would not be selected by traditional Lyman break criteria. Studying samples that are complete to a rest-frame optical limit, or to a stellar mass limit, implies a compromise: one either works with small, bright samples for which it is possible to obtain spectra (Cimatti et al. 2002; Kriek et al. 2008), or one relies on photometric redshifts derived from broad-band photometry (e.g., Dickinson et al. 2003; Fontana et al. 2006, and many other studies). These photometric redshifts are generally assumed to be sufficiently accurate for determining broad characteristics of the galaxy population, such as the luminosity function. However, redshift errors can lead to biases (see, e.g., Marchesini et al. 2007, Reddy et al. 2008), and these redshifts cannot be used to measure accurate rest-frame colors, stellar population parameters, or the local galaxy density. Furthermore, their random errors typically have a non-Gaussian distribution (leading to so-called ‘‘catastrophic failures’’) and they can have significant systematic uncertainties (see, e.g., Brammer et al. 2008, and references therein).

Inspired by the successful COMBO-17 optical medium-band imaging survey at redshifts $0 < z < 1$ (Wolf et al. 2003), we are undertaking a project which will provide a sample of K -selected galaxies with accurate redshifts in the range $1.5 < z < 3.5$ that is several orders of magnitude larger than what is available today. We designed and manufactured a set of five medium-bandwidth near-infrared (near-IR) filters, which provide ‘‘spectra’’ with a resolution of $R \sim 10$ from $1 - 1.8 \mu\text{m}$. The filters are designed to isolate the location of the redshifted Balmer- or 4000 \AA -break for galaxies at $1.5 < z < 3.5$. A set of these filters was manufactured for the NEWFIRM camera (Probst et al. 2004) on the Kitt Peak 4m, and the NEWFIRM Medium Band Survey (NMBS; an NOAO Survey Program) began in March 2008. This paper describes the characteristics of the filters, outlines the survey strategy, and shows results from a short pilot program that we executed in the Spring of 2008. The survey will be described more extensively in a forthcoming paper (K. Whitaker et al., in preparation).

2. Filter Characteristics

The filters are shown in Fig. 1. The J band is split in three filters J_1 , J_2 , and J_3 , and the H band is split in two filters H_1 and H_2 . Each filter consists of two physically separate components: a transmission filter and a blocking filter, which both need to be mounted in the two filter wheels of NEWFIRM. The blocking filters are needed because of the long-wavelength sensitivity of NEWFIRM’s InSb arrays, and are the cause of the ‘‘roll-off’’ in sensitivity toward shorter wavelengths and the wiggles in the transmission curves of (particularly) J_2 and J_3 . The J_1 filter has its own blocking filter, J_2 and J_3 share a blocking filter, and H_1 and H_2 share a blocking filter. Mounting all five filters in NEWFIRM therefore requires eight filter slots.

Central wavelengths and 50% cut-on and cut-off wavelengths for the five filters are listed in Table 1. The J_1 filter is somewhat redder and broader than the Y filter used by, e.g., the UKIRT Infrared Deep Sky Survey, whose cut-on and cut-off wavelengths are $0.97 \mu\text{m}$ and $1.07 \mu\text{m}$ respectively. The J_3 filter is narrower and redder than the J_s (‘‘ J -short’’) filter used in, e.g., HAWK-I on the Very Large Telescope. The wavelength range covered by the J_2 filter contains an atmospheric H_2O absorption feature, and the red edge of the J_3 filter pushes slightly into the H_2O band between the J and H windows. The atmosphere leads to a decrease in throughput of up to $\approx 10\%$ in the J_2 and J_3 filters. Figure 1 and Table 1 demonstrate the effects of varying the H_2O column between 1.6 mm and 3.0 mm; for all filters the variations in throughput due to variations in the water column are $\lesssim 2\%$.

Table 1: Basic Filter Data

	J_1	J_2	J_3	H_1	H_2
λ_{cen}^a	1.047	1.195	1.279	1.560	1.708
λ_{blue}^b	0.969	1.115	1.209	1.474	1.621
λ_{red}^b	1.120	1.263	1.350	1.641	1.796
$T_{1.6\text{mm}}^c$	0.98	0.94	0.92	0.97	0.97
$T_{3.0\text{mm}}^c$	0.97	0.92	0.90	0.96	0.96
ΔAB^d	0.65	0.84	0.96	1.29	1.42

^aIncludes atmosphere, with 3.0 mm water column.

^b50% cuton/cutoff wavelengths; includes atmosphere.

^cTransmission of the atmosphere for different water columns.

^dSynthetic AB magnitudes of Vega.

Transformations from the Vega to the AB system were calculated by integrating the Vega spectrum, using filter curves that include atmospheric absorption.

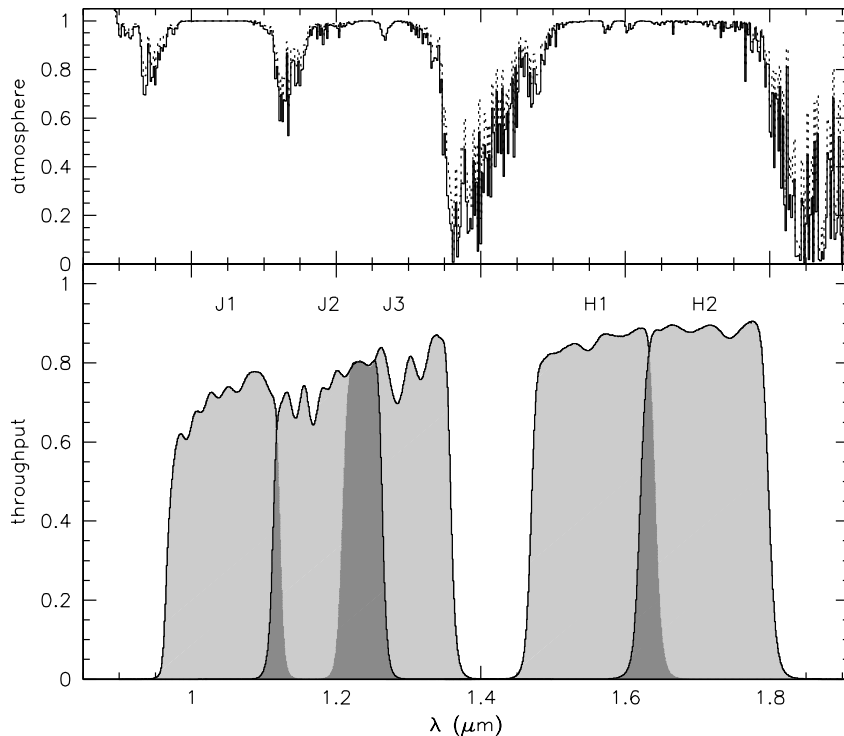


Fig. 1.— Medium-bandwidth filters designed for NEWFIRM and used in the NMBS. The throughput of the filters ranges from $\approx 70\%$ for J_1 to $\approx 90\%$ for H_2 (excluding effects of the atmosphere). The top panel shows the atmospheric transmission spectrum, for two different water columns: the broken line is for a column of 1.6 mm and the solid line is for 3.0 mm.

The uncertainties in the AB offsets listed in Table 1 are ≈ 0.02 , and are dominated by uncertainties in the absolute calibration of Vega.

3. Survey Strategy

The goal of the NMBS is to obtain high-quality SEDs and redshifts for galaxies down to a limit of $K \approx 21.5$. In practice, we aim to secure medium-band photometry with a 1σ uncertainty of $\approx 2 \times 10^{-20}$ ergs s^{-1} cm^{-2} \AA^{-1} . This constant limit in F_λ should provide $> 8\sigma$ photometry in bands redward of the Balmer break for most galaxies with $1.5 < z < 3.5$ and $K < 21.5$ (Vega; $K_{AB} < 23.3$). This limit allows us to select and study samples that are $> 95\%$ complete for galaxies with stellar masses $> 10^{11} M_\odot$ out to $z \sim 3$ (van Dokkum et al. 2006). The required integration times strongly depend on conditions, and are typically ~ 40 hrs per band.

We are targeting two fields: a single $27'.6 \times 27'.6$ NEWFIRM pointing within the COSMOS field (Scoville et al. 2007) and a single pointing overlapping with

part of the AEGIS strip (Davis et al. 2007). The center of the COSMOS pointing is at $\alpha = 9^h 59^m 53.3^s$, $\delta = +02^\circ 24' 08''$ (J2000); it overlaps with the extensive datasets at other wavelengths that are available for this field, including the zCOSMOS deep redshift survey (Lilly et al. 2007) and the upcoming UltraVISTA survey⁸. The AEGIS pointing is centered at $\alpha = 14^h 18^m 00^s$, $\delta = +52^\circ 36' 07''$ (J2000). It overlaps with about 50% of the deep ACS and Spitzer imaging in AEGIS and with the “Westphal” field, which contains 188 spectroscopically confirmed Lyman break galaxies (see Steidel et al. 2003). For both fields public optical *ugriz* data are available from the Deep Canada-France-Hawaii Telescope Legacy Survey⁹. These data are of uniform quality (at least over the extent of the NEWFIRM fields) and very deep, reaching typical 10σ AB limits of ~ 25.5 for point sources.

These two fields are observed whenever they are

⁸<http://www.eso.org/sci/observing/policies/PublicSurveys/>

⁹<http://www.cfht.hawaii.edu/Science/CFHTLS/>

Table 2: Spectrophotometric Standards^a

ID	α	δ	J_1	J_2	J_3	H_1	H_2	K
G191B2B	05 ^h 05 ^m 30.6 ^s	+52 ^o 49 ^m 53.6 ^s	12.44	12.52	12.54	12.62	12.67	12.75
GD71	05 ^h 52 ^m 27.5 ^s	+15 ^o 53 ^m 16.6 ^s	13.66	13.72	13.75	13.82	13.87	13.95
GD153	12 ^h 57 ^m 02.4 ^s	+22 ^o 01 ^m 56.0 ^s	13.99	14.06	14.09	14.16	14.21	14.29
P041C	14 ^h 51 ^m 57.9 ^s	+71 ^o 43 ^m 13.0 ^s	11.08	10.94	10.85	10.60	10.57	10.55
P177D	15 ^h 59 ^m 13.6 ^s	+47 ^o 36 ^m 40.0 ^s	12.49	12.33	12.22	11.96	11.92	11.90
P330E	16 ^h 31 ^m 33.6 ^s	+30 ^o 08 ^m 48.0 ^s	12.02	11.86	11.76	11.49	11.45	11.42
1740346	17 ^h 40 ^m 34.7 ^s	+65 ^o 27 ^m 15.0 ^s	12.18	12.12	12.09	12.02	12.02	11.99
1805292	18 ^h 05 ^m 29.3 ^s	+64 ^o 27 ^m 52.1 ^s	12.10	12.07	12.06	12.02	12.02	12.00
1812095	18 ^h 12 ^m 09.6 ^s	+63 ^o 29 ^m 42.3 ^s	11.43	11.39	11.37	11.31	11.30	11.28
KF06T1	17 ^h 57 ^m 58.5 ^s	+66 ^o 52 ^m 29.3 ^s	11.89	11.84	11.61	11.31	11.30	11.29

^aAll magnitudes are on the Vega system.

available and conditions are good. In mediocre conditions we observe backup fields to much shallower depth. The goal is to obtain several of these fields over the course of the survey, as they play an important role in calibrating photometric redshifts, constraining the bright end of the luminosity- and mass-functions, and in providing targets for follow-up spectroscopy. In the following we report on observations of the first of these backup fields, the MUSYC SDSS 1030+05 field.

4. Observations and Reduction of the MUSYC SDSS 1030+05 Field

The first run of the NMBS comprised a contiguous block of 24 nights, 2008 March 24 – April 16. A detailed description of the observations in our primary COSMOS and AEGIS fields will be presented in K. Whitaker et al., in preparation. Here we discuss observations in the bad weather backup field MUSYC SDSS 1030+05 (see Quadri et al. 2007; Blanc et al. 2008). This is one of the four 30' \times 30' fields surveyed by the MUltiwavelength Survey by Yale-Chile (MUSYC; Gawiser et al. 2006). It is centered on $\alpha = 10^h30^m27.1^s$, $\delta = +05^o24^m55^s$ (J2000), and contains the $z = 6.3$ QSO SDSSpJ1030027.10+052455.0 (Becker et al. 2001).

We chose this field because it contains 14 objects from a sample of spectroscopically-confirmed K -selected galaxies at $z \sim 2.3$ (Kriek et al. 2008). The Kriek et al. sample is unbiased with respect to observed-optical flux, as it was selected on the basis of K -magnitude and photometric redshift only. Furthermore, rest-frame optical continuum spectroscopy is available for the entire sample (see Kriek et al. 2008). The NMBS observations in this field therefore effec-

tively serve as a small pilot program, allowing us to assess whether the medium band filter technique can indeed provide reliable SEDs and redshifts for optically-faint sources. Even though there are thousands of spectroscopic redshifts available in our primary survey fields (AEGIS and COSMOS), they are almost exclusively for optically-bright, low redshift galaxies.

Because the SDSS 1030+05 field served as a bad weather backup field the data quality is relatively poor (as compared to the main survey fields). The seeing was typically in the range 1''4–1''8 when we observed the field, and the background was often relatively high. Total integration times were 2.3 hrs in J_1 , 1.1 hrs in J_2 , 2.5 hrs in J_3 , 1.1 hrs in H_1 , and 1.6 hrs in H_2 . The data were processed using a new reduction package, which was developed by one of us (IL). The heart of the code is similar to the popular IRAF XDIMSUM package, but it incorporates many of the changes that we have developed over the years (see Labbé et al. 2003; Quadri et al. 2007). The code was completely rewritten in the IDL programming environment, automated, and optimized for NEWFIRM.

The data were calibrated by repeated observations of six different near-IR spectrophotometric standards. Synthetic magnitudes of these stars were calculated by integrating their observed (HST/NICMOS) spectra in our filters. We verified that this method reproduces the (independently calibrated) broad-band J , H , and K band magnitudes of these stars. Based on the observed variation of zeropoints derived from different stars and on different photometric nights we estimate that the zeropoint uncertainties are $\lesssim 0.02$ mag. The stars and their synthetic magnitudes are listed in Table 2, along with stars that were not observed during

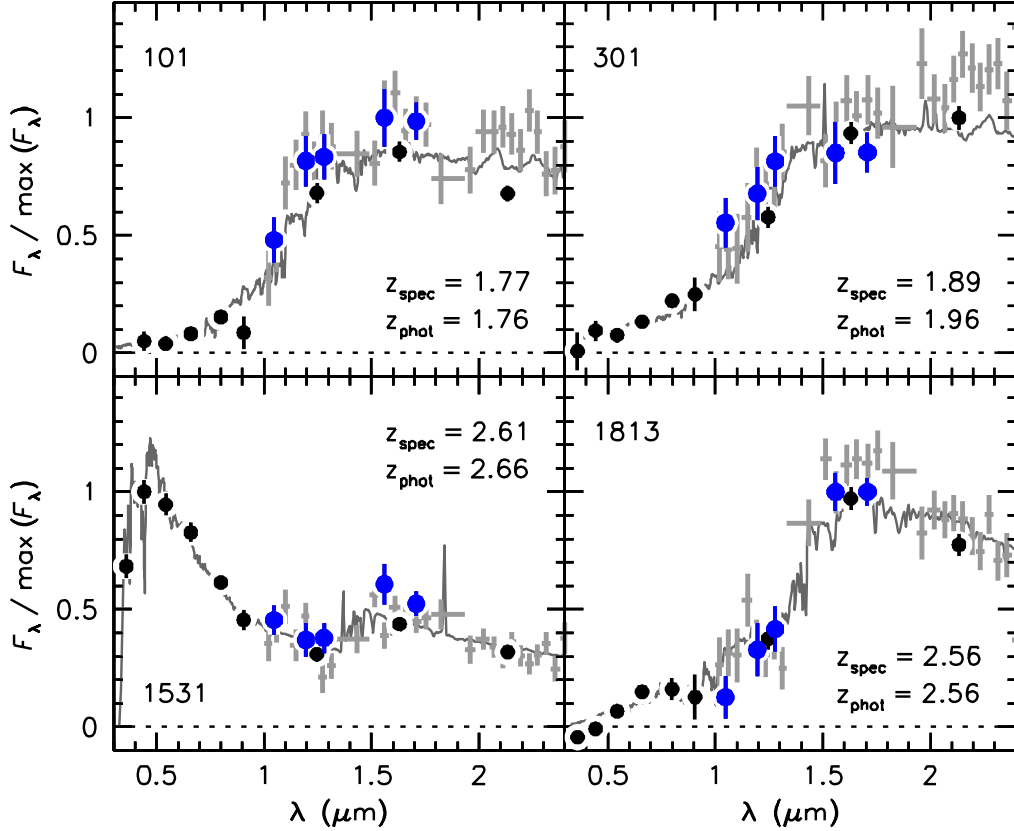


Fig. 2.— Spectral energy distributions from 0.3–2.4 μm of the four galaxies in the SDSS 1030 Kriek et al. (2008) sample with the highest S/N ratio. Black points are broad band photometric data, blue points are the new medium band data. The medium band data are able to pinpoint the location of rest-frame optical breaks in the spectra. Dark grey spectra are the best-fit EAZY model SEDs. Light grey points are binned near-IR spectra obtained with GNIRS on Gemini, from Kriek et al. The best-fit model SEDs fit the (independent!) GNIRS spectra very well.

the March/April run. The achieved 5σ depths in the SDSS 1030+05 field are $J_1 = 22.2$, $J_2 = 21.5$, $J_3 = 21.4$, $H_1 = 20.8$, and $H_2 = 20.9$ (total Vega magnitudes for point sources).

The medium-band images were combined with $UBVRIZK$ imaging from the MUSYC survey. A general description of the MUSYC optical imaging is given in Gawiser et al. (2006); specific aspects of the SDSS 1030 field are provided in Quadri et al. (2007) and Blanc et al. (2008). The methodology for PSF-matching of the optical- and near-IR data and the procedures for creating a K -selected catalog are the same as used in Labbé et al. (2003) and Quadri et al. (2007). We also included Spitzer IRAC imaging in the analysis, which are described in Marchesini et al. (2008). The IRAC data do not cover the full NEWFIRM field, but do cover the galaxies from the Kriek et al. (2008)

sample. The final product is a K -selected catalog with accurate $UBVRIZJ_1J_2J_3H_1H_2K$ +IRAC fluxes.

5. Results

5.1. Spectral Energy Distributions

Of the 14 galaxies in the SDSS 1030 field that overlap with the Kriek et al. (2008) sample, four have an average S/N ratio in the H_1 and H_2 filters which exceeds our survey criterion of 8. The broad + medium band photometry of these galaxies is shown in Fig. 2, along with the (binned) GNIRS spectra from Kriek et al. (2008) (shown in light grey).

The medium band photometry is consistent with both the GNIRS continuum spectroscopy and with the broad band J and H data. The medium bands sam-

ple the spectral energy distributions (SED) more finely than the broad bands, and capture the overall shape of the SEDs as traced by the GNIRS spectra. In particular, there are obvious breaks in the medium band photometry, making it possible to pinpoint the location of the redshifted Balmer- or 4000 Å break *within* the J band window (or between J_3 and H_1 for objects 1531 and 1813). This is a significant advance: the medium bands sample the SED with a spectral resolution of $R = 10\text{--}11$, whereas standard broad-band near-IR photometry corresponds to $R = 3\text{--}4$.

The ability to detect breaks obviously depends on a combination of the intrinsic strength of the break and the S/N ratio of the photometry. Galaxy 1813¹⁰ has a very strong break between J_3 and H_1 , which would also have been detected in shallower exposures. The breaks in the other galaxies are weaker, and the ability to measure accurate redshifts will depend sensitively on the quality of the photometry. The average S/N ratio in H_1 and H_2 ranges from 8 to 15 for the four galaxies shown in Fig. 2; the goal of the main survey is to reach a S/N ratio > 8 in the bands redwards of $\lambda_{\text{rest}} = 4000 \text{ \AA}$ for galaxies with $K < 21.5$ in our NEWFIRM fields.

5.2. Photometric Redshifts

Redshifts are measured with the photometric redshift code EAZY (Brammer et al. 2008), which is optimized for situations where complete spectroscopic calibration samples are not available. The default template set and rest-frame template error function were used, and the default magnitude and redshift priors (appropriate for the K band). Although not of great consequence in the present context, the “CHI2_SCALE” parameter was set to 0.5 in order to provide more realistic errorbars.¹¹

The photometric redshifts are compared to the Gemini/GNIRS redshifts from Kriek et al. (2008) in Fig. 3. There is excellent agreement for the four galaxies, with the biweight scatter in $(z_{\text{phot}} - z_{\text{spec}})/(1 + z_{\text{spec}})$ only 0.010. This value is not very robust given the small sample size (the normalized median absolute deviation is 0.020, and the rms is 0.011), but it is substantially better than what has so far been achieved at these redshifts. As an example, Grazian et al. (2007)

¹⁰The numbering follows Kriek et al. (2008), who give coordinates, K magnitudes, and other information for these galaxies.

¹¹We find that the default EAZY uncertainties slightly overestimate the errors; as discussed in Brammer et al. (2008) the exact interpretation of the uncertainties can vary between datasets.

and Brammer et al. (2008) find a scatter of 0.06 – 0.07 at $z > 1.5$ using state of the art broad-band data in the CDF-South field. Similarly, Ilbert et al. (2008) find a scatter of 0.06 (with 20% catastrophic outliers) at $1.5 < z < 3$ in COSMOS using 30 photometric bands (including GALEX, IRAC, and 18 medium-bandwidth optical filters from Subaru).

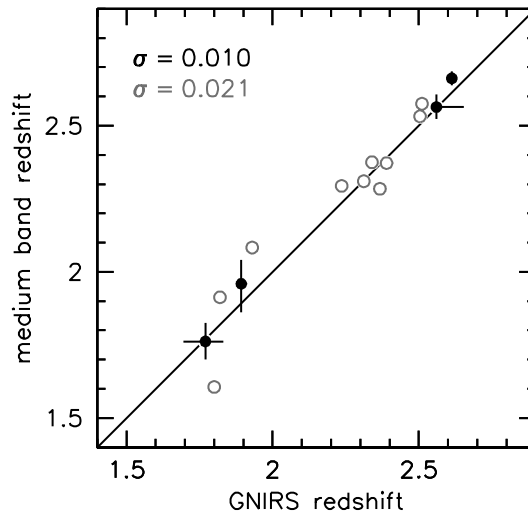


Fig. 3.— Comparison of photometric redshifts derived from medium band photometry to spectroscopic redshifts measured with the GNIRS near-IR spectrograph on Gemini for the four galaxies shown in Fig. 2 (solid symbols). There is very good agreement, with scatter 0.01–0.02 in $\Delta z/(1+z)$. Open symbols show the remaining 10 objects from the Kriek et al. (2008) sample. The scatter is small even for these galaxies, even though the S/N of their medium band photometry is lower than our survey criterion.

Open symbols in Fig. 3 have a S/N less than our survey criterion of 8 in the H_1 and H_2 bands. Interestingly, they nevertheless show relatively small scatter as well, and the scatter in the full sample of 14 galaxies is ≈ 0.023 in $\Delta z/(1+z)$. The sample is obviously too small to investigate the exact behavior of the redshift uncertainty as a function of S/N ratio, but the presently available information suggests that uncertainties of ≈ 0.02 in $\Delta z/(1+z)$ can be achieved with a S/N of 6–10 in filters redward of the redshifted Balmer/4000 Å break.

The dark grey spectra in Fig. 2 are the best-fitting EAZY templates.¹² These templates fit the observed photometry well, and all four galaxies have acceptable

¹²Each template is actually a linear combination of six “base” templates, and these six base templates are themselves linear combina-

best-fit χ^2 values (partly owing to the template error function; see Brammer et al. 2008). The dark grey model spectra fit the binned GNIRS spectra remarkably well; the only significant deviation is a $\approx 20\%$ underprediction of the flux at $\approx 2.2\ \mu\text{m}$ for galaxy 301.

6. Other Applications: Selecting the Coolest Brown Dwarfs

The medium-band filters were designed to improve redshift estimates and stellar population constraints for distant galaxies but can also be used for other purposes, in particular when used in a wide, relatively shallow survey. Among these other applications are the identification of objects with extremely bright emission lines; improved star/galaxy separation; identification and characterization of high redshift galaxies and QSOs; and finding cool brown dwarfs. In the following we expand on the latter application.

As illustrated for a T7 dwarf in Fig. 4 the spectra of very late type dwarfs (beyond the L/T boundary) are characterized by strong H_2O and CH_4 absorption. The subtype within the T class is determined by the strengths of these absorption bands, which in turn are thought to be closely correlated with the effective temperature (see Burgasser et al. 2002). The most dramatic change going from T1–T9 is in the broad methane absorption at $\sim 1.7\ \mu\text{m}$, which is weak at the L/T boundary and almost complete for the coolest T dwarfs.

Finding the coolest dwarfs typically involves a multi-stage process: the initial selection uses *JHK* photometry from 2MASS (e.g., Burgasser et al. 2002) or *iz* photometry from the CFHTLS (e.g., Delorme et al. 2008); follow-up broad-band near-IR imaging is used to weed out interlopers and spurious sources and to obtain accurate $J-H$ and $H-K$ colors; and near-IR spectroscopy provides the spectral type.

Interestingly, the medium band filters offer an extremely efficient way to select ultra-cool stars, as the H_2 filter coincides almost exactly with the location and width of the CH_4 feature at $\sim 1.7\ \mu\text{m}$. As a result, the H_1-H_2 color is a very strong function of spectral class (and hence effective temperature) for the coolest dwarfs. In Fig. 5 we show the relation between the H_1-H_2 color and spectral type for the T dwarfs of Burgasser et al. (2002). The colors are not based on

tions extracted from a large template library – see Brammer et al. (2008) for details.

models but were calculated by integrating the observed near-IR spectra of these dwarfs¹³.

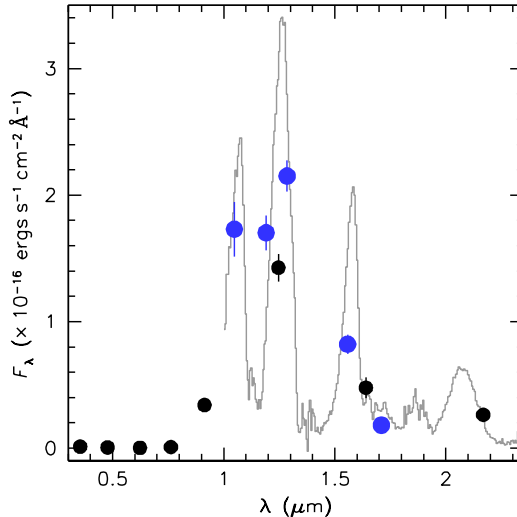


Fig. 4.— Observations in *ugrizJHK* (black) and the medium band filters (blue; obtained in twilight) for the T7 dwarf 2MASS 1553+1532. The spectrum is from Burgasser et al. (2002). This cool dwarf has a unique signature in the medium band filters, particularly in the H_1-H_2 color.

There is a clear relation between T subclass and H_1-H_2 color, with H_1-H_2 progressively bluer for later types. The relation shown by the broken line has the form $T_x = 4.2 - 2.7(H_1 - H_2)$; it has an rms of less than one subclass. The histogram shows the distribution of H_1-H_2 colors for all objects in the SDSS 1030 field. Normal stars and galaxies are well-separated from the coolest dwarfs, and Fig. 5 suggests that a simple selection on H_1-H_2 color (e.g., $H_1-H_2 < -1$) should yield a clean sample of very cool dwarfs.

It is interesting to speculate whether the H_1-H_2 color could also be used to select stars with $T_{\text{eff}} < 700\ \text{K}$, the elusive “Y” class (e.g., Kirkpatrick et al. 1999). The CH_4 band saturates near the T/Y boundary, which limits its utility for spectral classification. Nevertheless, the recently discovered T/Y transition object CFBDS J005910.90–011401.3 (Delorme et al. 2008) falls on the same relation as the late T dwarfs (see Fig. 5). It may therefore be possible to select Y dwarfs by the simple criterion $H_1-H_2 < -1.5$.

¹³Obtained from <http://web.mit.edu/ajb/www/tdwarf/#spectra>.

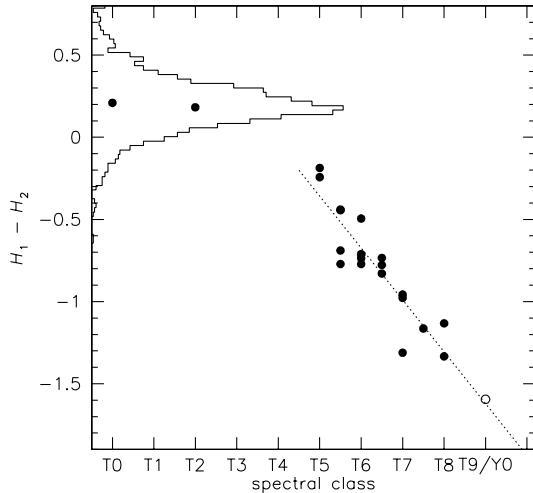


Fig. 5.— Relation between $H_1 - H_2$ color and T subclass, as derived from near-IR spectra of cool dwarfs from Burgasser et al. (2002). The histogram shows the distribution of $H_1 - H_2$ colors for all objects in the SDSS 1030 field; dwarfs with spectral type \gtrsim T5 can be uniquely identified by their extremely blue $H_1 - H_2$ color. Also included is the coolest dwarf known to date, which may be a T/Y boundary object (Delorme et al. 2008). This object falls on the same relation as the other T dwarfs.

7. Conclusions

We have developed a medium bandwidth filter system in the near-IR, providing a compromise between spectroscopy and broad-band imaging. Installed in the wide-field NEWFIRM camera on Kitt Peak, the filters enable us to obtain high quality redshifts and spectral energy distributions for large, complete samples of galaxies with far greater efficiency than is possible with spectroscopy. The NMBS aims to obtain redshifts of $\approx 40,000$ galaxies with $K < 21.5$, some 8000 of which are expected to be at $z > 1.5$. To put this in context, with a multi-object near-IR spectrograph such as FLAMINGOS-2 on Gemini it would require ~ 2500 hrs to obtain redshifts for 1000 galaxies to this limit (scaling from Kriek et al. 2008).

Although the initial results reported here are promising, the accuracy of the redshift measurements needs to be verified. The medium-band technique relies on the presence of a break in the rest-frame optical, and the improvement in photometric redshift estimates will therefore depend on galaxy type. Very young stellar populations with ages $\lesssim 300$ Myr do not have a significant Balmer break, and the accuracy of the redshifts

of many Lyman break and “BM/BX” galaxies (Steidel et al. 2004) may therefore not be much better than can be derived from broad-band optical photometry alone. Similarly, very dusty galaxies can have featureless red SEDs.

With larger samples of galaxies with spectroscopic redshifts we will be able to quantify these and other effects (such as the presence of bright emission lines, and the redshift-dependence of redshift errors). Such spectroscopic samples will obviously not be representative of our entire sample, but they can be used to assess the reliability of the uncertainties given by the EAZY code. If accuracies of 0.01 – 0.02 turn out to be typical for galaxies down to our survey limit, the NMBS will establish the relations between redshift, color, and density at $1.5 < z < 3.5$ with excellent statistics. Reduced images, catalogs, and derived redshifts, stellar population parameters, and rest-frame colors will be publicly released after the survey is completed. Finally, we note that the H_1 and H_2 filters enable very efficient searches for late T and candidate Y dwarfs.

We thank Ron Probst and the staff at NOAO for the construction of NEWFIRM and for their extensive help with, and enthusiasm for, this project. Philippe Delorme and Linhua Jiang kindly made spectra available to us in digital form. Support from NSF CAREER grant AST-0449678 and from NSF grant AST-0807974 is gratefully acknowledged. We thank the anonymous referee for constructive comments which improved the manuscript.

REFERENCES

- Becker, R. H., Fan, X., White, R. L., Strauss, M. A., Narayanan, V. K., Lupton, R. H., Gunn, J. E., & ETAL, X. 2001, *AJ*, 122, 2850
- Blain, A. W., Smail, I., Ivison, R. J., Kneib, J.-P., & Frayer, D. T. 2002, *Phys. Rep.*, 369, 111
- Blanc, G. A., Lira, P., Barrientos, L. F., Aguirre, P., Francke, H., Taylor, E. N., Quadri, R., Marchesini, D., et al. 2008, *ApJ*, 681, 1099
- Brammer, G. B., van Dokkum, P. G., & Coppi, P. 2008, *ApJ*, in press (arXiv:0807.1533)
- Burgasser, A. J., Kirkpatrick, J. D., Brown, M. E., Reid, I. N., Burrows, A., Liebert, J., Matthews, K., Gizis, J. E., et al. 2002, *ApJ*, 564, 421
- Cimatti, A., Mignoli, M., Daddi, E., Pozzetti, L., Fontana, A., Saracco, P., Poli, F., Renzini, A., et

- al. 2002, *A&A*, 392, 395
- Cimatti, A., Cassata, P., Pozzetti, L., Kurk, J., Mignoli, M., Renzini, A., Daddi, E., Bolzonella, M., et al. 2008, *A&A*, 482, 21
- Daddi, E., Alexander, D. M., Dickinson, M., Gilli, R., Renzini, A., Elbaz, D., Cimatti, A., Chary, R., et al. 2007, *ApJ*, 670, 173
- Davis, M., Guhathakurta, P., Konidaris, N. P., Newman, J. A., Ashby, M. L. N., Biggs, A. D., Barmby, P., Bundy, K., et al. 2007, *ApJ*, 660, L1
- Delorme, P., Delfosse, X., Albert, L., Artigau, E., Forveille, T., Rey, C., Allard, F., Homeier, D., et al. 2008, *A&A*, 482, 961
- Dickinson, M., Papovich, C., Ferguson, H. C., & Budavári, T. 2003, *ApJ*, 587, 25
- Fontana, A., Salimbeni, S., Grazian, A., Giallongo, E., Pentericci, L., Nonino, M., Fontanot, F., Menci, N., et al. 2006, *A&A*, 459, 745
- Gawiser, E., van Dokkum, P. G., Herrera, D., Maza, J., Castander, F. J., Infante, L., Lira, P., Quadri, R., et al. 2006, *ApJS*, 162, 1
- Ilbert, O., Capak, P., Salvato, M., Aussel, H., McCracken, H. J., Sanders, D. B., Scoville, N., Kartaltepe, J., et al. 2008, *ApJ*, in press (arXiv:0809.2101)
- Kirkpatrick, J. D., Reid, I. N., Liebert, J., Cutri, R. M., Nelson, B., Beichman, C. A., Dahn, C. C., Monet, D. G., et al. 1999, *ApJ*, 519, 802
- Kriek, M., van Dokkum, P., Franx, M., Förster Schreiber, N., Gawiser, E., Illingworth, G., Labbe, I., Marchesini, D., et al. 2006, *ApJ*, 649, L71
- Kriek, M., van Dokkum, P. G., Franx, M., Illingworth, G. D., Marchesini, D., Quadri, R., Rudnick, G., Taylor, E. N., et al. 2008, *ApJ*, 677, 219
- Labbé, I., Franx, M., Rudnick, G., Schreiber, N. M. F., Rix, H., Moorwood, A., van Dokkum, P. G., van der Werf, P., et al. 2003, *AJ*, 125, 1107
- Lilly, S. J., Le Fèvre, O., Renzini, A., Zamorani, G., Scodreggio, M., Contini, T., Carollo, C. M., Hasinger, G., et al. 2007, *ApJS*, 172, 70
- Marchesini, D., van Dokkum, P., Quadri, R., Rudnick, G., Franx, M., Lira, P., Wuyts, S., Gawiser, E., et al. 2007, *ApJ*, 656, 42
- Marchesini, D., van Dokkum, P. G., Förster Schreiber, N. M., Franx, M., Labbé, I., & Wuyts, S. 2008, *ApJ*, in press (arXiv:0811.1773)
- Probst, R. G., Gaughan, N., Abraham, M., Andrew, J., Daly, P., Hileman, E., Hunten, M., Liang, M., et al. 2004, *SPIE*, 5492, 1716
- Quadri, R., Marchesini, D., van Dokkum, P., Gawiser, E., Franx, M., Lira, P., Rudnick, G., Urry, C. M., et al. 2007, *AJ*, 134, 1103
- Reddy, N. A., Steidel, C. C., Pettini, M., Adelberger, K. L., Shalpey, A. E., Erb, D. K., & Dickinson, M. 2008, *ApJS*, 175, 48
- Scoville, N., Aussel, H., Brusa, M., Capak, P., Carollo, C. M., Elvis, M., Giavalisco, M., Guzzo, L., et al. 2007, *ApJS*, 172, 1
- Steidel, C.-C., Shalpey, A. E., Pettini, M., Adelberger, K. L., Erb, D. K., Reddy, N. A., & Hunt, M. P. 2004, *ApJ*, 604, 534
- Steidel, C. C., Adelberger, K. L., Giavalisco, M., Dickinson, M., & Pettini, M. 1999, *ApJ*, 519, 1
- Steidel, C. C., Adelberger, K. L., Shalpey, A. E., Pettini, M., Dickinson, M., & Giavalisco, M. 2003, *ApJ*, 592, 728
- Steidel, C. C., Giavalisco, M., Pettini, M., Dickinson, M., & Adelberger, K. L. 1996, *ApJ*, 462, L17
- Trujillo, I., Förster Schreiber, N. M., Rudnick, G., Barden, M., Franx, M., Rix, H.-W., Caldwell, J. A. R., McIntosh, D. H., et al. 2006, *ApJ*, 650, 18
- van Dokkum, P. G., Franx, M., Kriek, M., Holden, B., Illingworth, G. D., Magee, D., Bouwens, R., Marchesini, D., et al. 2008, *ApJ*, 677, L5
- van Dokkum, P. G., Quadri, R., Marchesini, D., Rudnick, G., Franx, M., Gawiser, E., Herrera, D., Wuyts, S., et al. 2006, *ApJ*, 638, L59
- Wolf, C., Meisenheimer, K., Rix, H.-W., Borch, A., Dye, S., & Kleinheinrich, M. 2003, *A&A*, 401, 73